to the corrected mean power spectra which result from all but one combinations between 3 sets of observations of R Dor and 4 sets of reference-star observations. There is no significant indication of a deviation from circular symmetry of more than 2 per cent. Smaller deviations are easily explained by residual artifacts in the visibility data.

Figure 2 shows radial plots (averages over the azimuth) of the compensated spectra. The black, heavy dots are the azimuth averages of the R Dor spectra. The origin of the dip near 1 lp/arcsec may be related to seeing variations; this region was excluded from the fitting process. The red curve shows the average and the variation of the non-linear fits to the data. The green, open circles show azimuth averages of inter-calibrated reference data to demonstrate the significance of the R Dor measurements.

The observed angular diameter of an M star can be strongly affected by the atmospheric extensions. Within bands of high opacity (such as the TiO bands) the star can appear 50 per cent larger than in continuum regions of the spectrum. It is therefore important to compare diameters for different stars only for measurements made in the continuum. A limb-darkening correction may also have to be applied, but this correction is somewhat ad-hoc due to the lack of reliable model atmospheres. Opacity effects and limb darkening are smallest in the infrared and stellar diameter measurements should preferably be taken in this region of the spectrum.

The uniform-disk diameter of Betelgeuse at 2.2 microns has been measured to be 44 mas (Dyck et al., 1992). Thus, R Dor appears to be the largest star in the sky.

Despite its classification as semi-regular, R Dor is in many ways closer to the Miras than to other SRb stars. Its period is near the peak of the Mira period distribution function (250–350 days), while SRb stars almost always have much shorter periods (e.g., Kerschbaum & Hron, 1992). Its late spectral type and large J–K are also more typical of Miras than other M-type stars (Feast, 1996). Using a bolometric magnitude at the epoch of our measurement of –0.96, we derive an effective temperature of 2740 ± 190 K from the measured diameter. Assuming that R Dor is closely related to the Mira variables, as seems likely, we can apply the period-luminosity relations for Miras in the LMC given by Feast 1996. We obtain a distance of 61 ± 7 pc and a luminosity for R Dor of 6500 ± 400 $L_\odot$. Our distance for R Dor agrees with estimates of 60 pc by Judge & Stencel, 1991, and 51 pc by Celis, 1995. This distance, together with our observed angular diameter, implies a stellar radius of 370 ± 50 $L_\odot$. From the pulsation equation $\bar{Q} = \bar{P}\,(\bar{M}/M_\odot)^{1/2}\,(\bar{R}/R_\odot)^{-3/2}$ and assuming Q = 0.04 days (appropriate for first overtone pulsation), we derive a mass of 0.7 ± 0.3 $M_\odot$. All the derived parameters are consistent with a classification of this star as Mira-like, with the effective temperature being slightly higher than the average for Miras.

All previous measurements of the radii of Miras fall in the range 400–500 $R_\odot$, which is taken by Haniff et al., 1995, as evidence that Miras are associated with a well-defined instability strip. The fact that R Dor shows a more irregular pulsation behaviour but with many characteristics of a Mira is consistent with it lying near the edge of such a strip. Miras have been found to show surface structures and/or ellipticity: if R Dor is related to the Miras, it may be expected that it also shows these effects. MAPPIT/AAT observations of R Dor indeed show non-zero closure phases, indicative of asymmetries or surface structure. R Dor is clearly an excellent candidate for more detailed observations with the VLT and VLTI.

References

Bedding T.R., von der Lühe O., Zijlstra A.A., Eckart A., Tacconi-Garman L.E., 1993, *The Messenger*, **74**, 2.

Buscher D.F., Haniff C.-A., Baldwin J.-E., Warner P.J., 1990, *MNRAS*, **245**, 7P.

Celis S.L., 1995, *ApJS*, **98**, 701.

Dyck H.M., Benson J.A., Ridgway S.T., Dixon D.J., 1992, *AJ*, **104**, 1982.

Feast M.W., 1996, *MNRAS*, **278**, 11.

Haniff C.A., 1994, in Robertson J.G., Tango W.J. (eds.), *IAU Symposium 158: Very High Angular Resolution Imaging,* p. 317, Kluwer: Dordrecht.

Judge P.G., Stencel R.E., 1991, *ApJ*, **371**, 357.

Kerschbaum F., Hron J., 1992, *A&A*, **263**, 97.

Michelson Pease, 1921, *ApJ*, **53**, 249.

Tuthill P.G., Haniff C.A., Baldwin J.E., 1994a, in Robertson J.G., Tango W.J. (eds.), *IAU Symposium 158: Very High Angular Resolution Imaging,* p. 395, Kluwer: Dordrecht.

Tuthill P.G., Haniff C.A., Baldwin J.E., Feast M.W., 1994b, *MNRAS*, **266**, 745.

Wilson R.W., Baldwin J.E., Buscher D.F., Warner P.J., 1992, *MNRAS*, **257**, 369.

Wing R.F., 1971, *PASP*, **83**, 301.

Molecular Hydrogen Towards T Tauri Observed with Adaptive Optics

A. QUIRRENBACH, Max-Planck-Institut für Extraterrestrische Physik, Garching
H. ZINNECKER, Astrophysikalisches Institut, Potsdam

1. Introduction

Although T Tauri is the prototype of a large class of pre-main-sequence objects (the T Tauri stars), it is actually very peculiar. First, the optical primary (T Tau N) has an infrared companion (T Tau S) at a separation of ∼ 0.7″, which is completely obscured at visible wavelengths, but may dominate the bolometric luminosity of the system (Dyck et al., 1982, Ghez et al., 1991). Infrared companions have been found near a number of other pre-main-sequence stars, but their presence seems to be the exception rather than the rule (Zinnecker and Wilking, 1992). Second, and even more surprisingly, strong extended 2.121 μm H_2 (v = 1 – 0) S(1) rovibrational emission was found from T Tau (Beckwith et al., 1978). Despite extensive searches, H_2 emission with comparable strength has been found in very few other pre-main-sequence stars (e.g. Carr, 1990). Finally, there are two Herbig-Haro objects at right angles associated with T Tau (Schwartz, 1975, Bührke et al., 1986), giving rise to the suspicion that two misaligned pairs of jets emanate from the two components of the binary.

Taking a closer look at the environment of T Tau, and at the relation of the gas to the two stellar components requires spectral line imaging with the highest possible angular resolution. Van Langevelde et al. (1994) present an image of T Tau in the H_2 (v = 1 – 0) S(1) line with a resolution of 0.8″, but the central region of this image had to be blanked because of saturation[1]. More recently, Herbst et al. (1996) observed T Tau with the MPE imaging spectrometer 3D; these observations cover a field of 8″ × 8″ with a resolution of ∼ 0.7″. A complicated structure was detected on this scale, which was interpreted as an

[1]Note that Figure 1 in van Langevelde et al. (1994) is labelled incorrectly. The correct image size is ∼ 26″, rather than ∼ 52″.

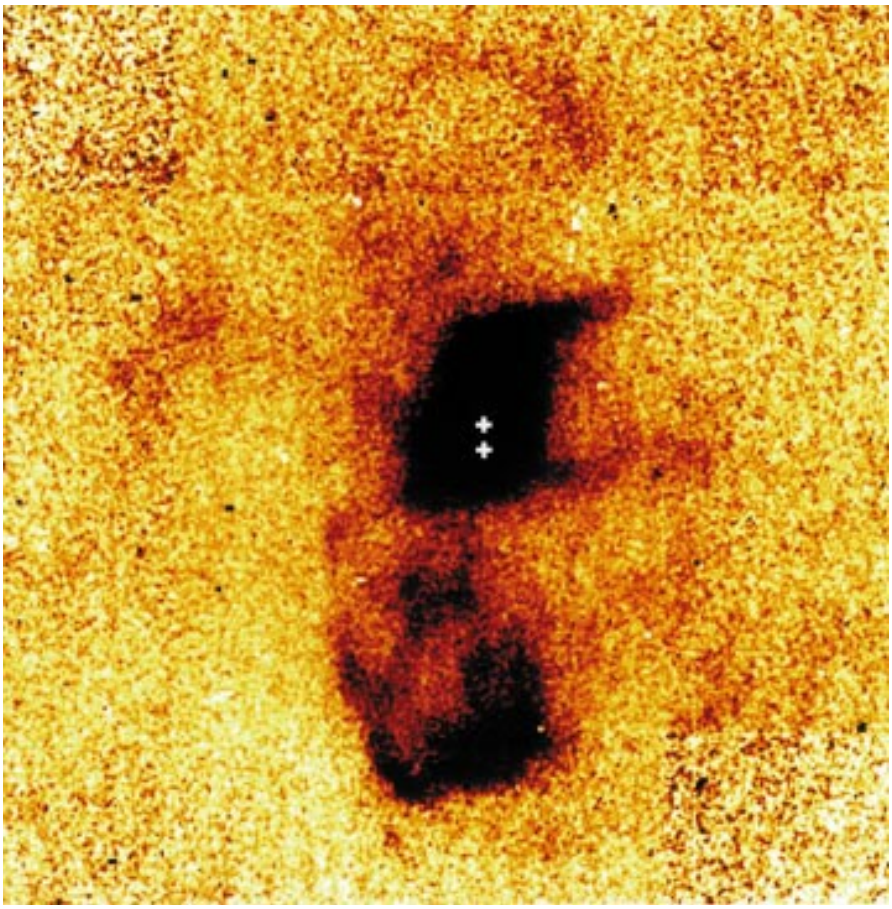

Figure 1: 2.121 μm H_2 (v = 1 – 0) S(1) ro-vibrational emission towards T Tauri. The field size is 25″ × 25″, North is up, and East is left. The positions of the two components of the T Tauri binary are marked with crosses. The continuum emission has been subtracted. The colour table has been chosen to emphasise low surface brightness emission. The most prominent features are the central "Z"-shaped emission region, and the complex structure in the south towards Burnham's nebula. In the north, a faint arc is seen at a position nearly mirror-symmetric to Burnham's nebula. In addition, three filaments are seen extending from the NW tip of the "Z", from its SW corner, and from its eastern side.

indication for two outflow systems, one of them oriented roughly N-S and associated with T Tau N, the other at a nearly perpendicular direction and emanating from the infrared companion. To test this picture, and to get even more detailed information, higher angular resolution is required, which provided the motivation for our adaptive optics observations.

2. Observations and Data Analysis

T Tauri was observed in the (v = 1 – 0) S(1) transition of molecular hydrogen at 2.121 μm with the SHARP II camera attached to the ADONIS adaptive optics system on January 15, 1996. To obtain optimum contrast between the faint line emission and the bright background from the stellar continuum and from the sky, it is necessary to use high spectral resolution. Therefore, we did not use an H_2 line filter, but rather SHARP II's high-resolution Fabry-Perot etalon, which provides a spectral resolution $R \sim 2500$ (i.e. ∼ 120 km/s). With an image scale of 0.1″ per pixel, we could cover a field of 25″ in each exposure. Positioning T Tauri successively in the four quadrants of the detector, we obtained a small 35″ × 35″ mosaic centred on the star.

Each data set contains a short sequence of two observations at the wavelength of the emission line, bracketed by two frames in the adjacent continuum at –600 km/s and +600 km/s, respectively. On the one hand, it is desirable to execute these Fabry-Perot sequences as quickly as possible, to minimise the seeing variations between the line and continuum images. On the other hand, with the relatively small pixel scale and the high spectral resolution of our observations, detector noise dominates over the sky background for integration times up to several minutes, which calls for long exposures. As a compromise between these conflicting requirements, we settled for a frame integration time of 60 seconds. On January 15, 1996, we spent a total of 20 minutes integrating on the 2.121 μm line in ∼ 0.7″ seeing. The results from these observations are presented here; additional data taken on the previous day in substantially poorer seeing (1.4″ to 1.9″) were discarded.

The raw data were corrected for bad pixels and flatfielded with exposures of the sky taken before sunset. (Because of strong wavelength-dependent fringes caused by interference in the detector substrate and the circular variable filter (CVF), which is used as an order sorter, we took sky flats at exactly the same wavelengths that we used for the astronomical observations.) All images were then resampled on a 0.05″ grid and recentred, before the continuum frames were subtracted from the line exposures. It turned out that this procedure did not only remove the continuum light from the stars, but it also resulted in an excellent cancellation of the sky background, because of the small wavelength difference between the line and continuum channels. The resulting images were coadded to form the final image of the v = 1 – 0 S(1) transition of H_2 towards T Tauri (see Figs. 1 and 2).

3. The Morphology of the 2.121 μm H_2 Emission Towards T Tauri

Perhaps the most striking property of the H_2 emission from the T Tau system is its unusual complexity. This may be partly due to the presumed nearly pole-on orientation, which would cause polar outflows and material in the equatorial plane to be projected on top of each other, and bends and misalignments to be exaggerated by projection effects. Therefore, we start with a purely morphological description of the results of our observations, before we proceed with the interpretation.

First, we are interested in the question whether most of the bright H_2 emission from the innermost star is associated with the visual primary or with the infrared companion. While observations with a scanning Fabry-Perot, in which line and continuum data are not taken simultaneously, are not optimum for the detection of line emission close to bright continuum sources, Figure 2 suggests that most of the compact H_2 emission comes from the infrared companion and that the emission region is resolved in the east-west direction. The next obvious features are a very bright knot 2– 3″ NW of the primary and an elongated filament at a position angle of ∼ 290° (measured from N through E) extending from this knot. A second filament with nearly the same orientation is seen 4.5″ further south, apparently pointing towards a position 0.7″ south of the IR companion. A third filament at position angle 60° is found in the east, connecting another bright knot 1.5″ east of the stars with an extended region of enhanced emission 9″ to the east. It should be pointed out that none of the filaments appears to be pointing back to either of the stellar components. A complex re-

gion of fairly bright hydrogen emission lies 4″ to 10″ south of the stars, towards Burnham's nebula. This emission region contains several knots and filaments; it appears to end abruptly in a bright southern rim. A corresponding, albeit much weaker, structure can be seen faintly in the north. It is worth noting that these features are all present at lower resolution in the lowest contours of Figure 1 in van Langevelde et al. (1994); this gives us confidence that they are all real. The bright NW knot, the western filament, and the northernmost knots of the southern emission region were also detected by Herbst et al. (1996).

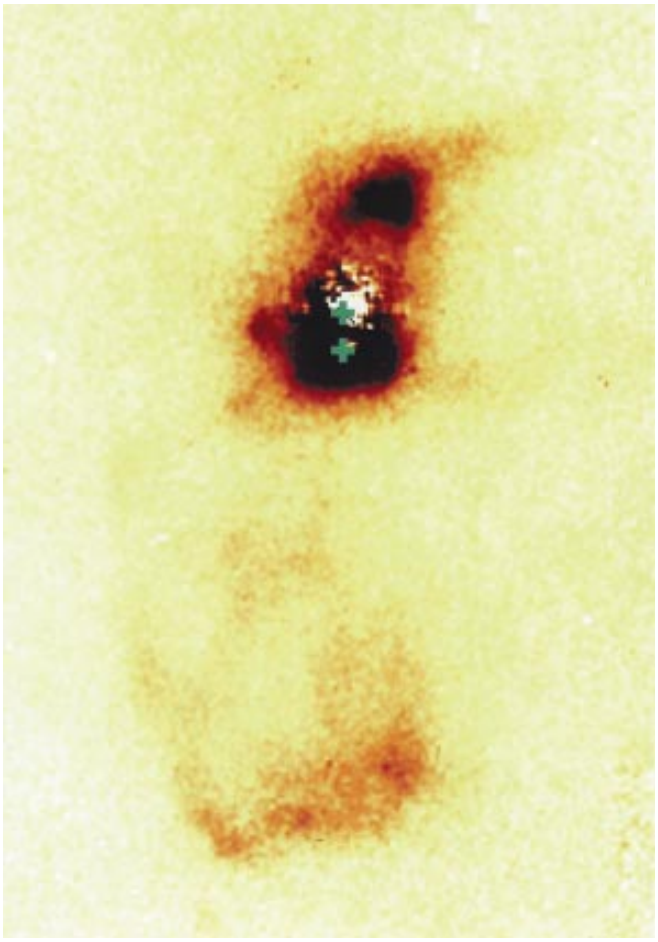

Figure 2: Same as Figure 1, but 12.5″ × 18″ field and different colour table. Artefacts from the non-perfect continuum subtraction are seen at the positions of the stars, but it is obvious that most of the compact H_2 emission is associated with the southern (IR) component. Two bright knots, which are well detached from the stars, are visible in the NW and E, at the footpoints of filaments 1 and 3. The complex structure in the south ends abruptly in a bright rim.

4. Interpretation

The H_2 data are suggestive of at least one collimated outflow in the T Tau system, roughly in the north-south direction: Burnham's nebula a few arcsec to the south of T Tau appears as a bright bow-shock projected close to the line of sight, while its arc-like counterpart symmetrically placed a few arcsec to the north of T Tau appears much fainter. This flow direction is about the same as the direction of the superjet seen in Hα as a series of 3 bow-shocks north and south of T Tau up to a distance of 20′ (1 pc) from the source (Reipurth, Bally, & Devine, in preparation). It is not clear whether the collimated flow traced in H_2 originates from T Tau N (the optical star) or T Tau S (the IR companion). On one hand, Solf et al. (1988) have found a jump in velocity in [SII] emission on the optical star, interpreted as a jet-like feature. On the other hand, the generally presumed connection between accretion and ejection tends to favour the IR companion as the jet source, as IR companions are considered as temporary accretors (Koresko et al., 1997). Herbst et al. (1996) argue that there are two outflow systems, one of them comprised by the NW knot and the southern emission region, and the other one by the SW and E filaments. Our finding that none of the filaments seems to emanate from either star, and the detection of an apparent counter-structure to Burnham's nebula, appear to contradict this picture. However, it must be kept in mind that precession and motion of the jet footpoints in the binary system might lead to strong bends and misalignments. Furthermore, the near-IR emission traces shocked hydrogen and not the bulk of the material, which may render the observed morphology misleading.

The fact that it is the IR companion rather than the optical star on which the H_2 emission is concentrated is taken to imply that matter is falling onto the circumstellar disk of the IR companion whereby it is shock-excited. Infall velocities of the order of 5–10 km/s are needed to produce the H_2 v = 1 – 0 excitation around 2000 K (Smith & Brand, 1990). This infall could arise from the inner edge of a circumbinary disk (Artymowicz & Lubow, 1996), which is detected both in CO interferometric observations (Weintraub et al., 1989, Momose et al., 1996) and in scattered IR light (Weintraub et al., 1992). There is no question that a fair amount of dusty disk and envelope gas (of the order of 0.01 $M_\odot$) likely to be bound to T Tau is present.

There are more H_2 features in our map than can be explained by H_2 jets. The filaments or fingers (one to the east and two to the west) may have nothing to do with jets whatsoever but rather come from material in the equatorial (disk) plane. We suggest two possible alternative origins for these features:

(1) Tidal tails caused by the interaction of the two star-disk systems (T Tau N and T Tau S), much like in interacting disk galaxy pairs. In this case, the expected shock velocities are of the order of the Keplerian orbital velocity of the binary system (around 5 km/s).

(2) Spiral shocks in the circumbinary disk of the T Tau binary system. These would arise as the binary drives spiral waves into the circumbinary disk with a pattern speed of the order of the orbital speed (5 km/s). Although the gas in the circumbinary disk has only a small orbital velocity (less than 1 km/s at radial distances in excess of 300 AU), the gas could be shock excited to emit in H_2, while running into the externally excited spiral potential well with a difference speed of a few km/s. These spiral shocks could be associated with accretion streams from the inner edge of the circumbinary disk, which also cause the shock excitation of the H_2 in the circumstellar disks.

Finally let us discuss the origin of the bright H_2 knot 2–3″ NW of T Tau N. We speculate that it might be related to a spiral shock which might be strongest right at the inner edge of the circumbinary disk. It is likely a density enhancement, because this knot is also visible in coronographic I-band images (Nakajima & Golimowski, 1995) as a reflection nebula (also seen in Hα but not in [SII], Robberto et al., 1995). It is noteworthy that the whole H_2 emission in the immediate vicinity of the binary system (including the NW knot and the IR companion and its respective H_2 fingers) are "Z" shaped as is the associated optical reflection nebula. Thus there is a strong similarity between dense gas and dust seen in reflected optical light and shocked H_2 emission, which has not been noticed before. Perhaps this could indicate some shock interaction of a diffuse outflow with the remnant material in the circumbinary environment.

In summary, we stress that the H_2 features seen in the T Tau system very

likely have different origins. The fact that the T Tau system is almost unique in showing extended H_2 emission could (a) be related to the presence of a jet interacting with the local environment (Burnham's Nebula and its northern counterpart), and (b) be related to a relatively massive circumbinary disk and a binary system with a component orbital speed of the same order as is necessary to shock excite molecular hydrogen (5 km/s) in this disk.

5. Future Prospects

The high angular resolution afforded by SHARP II and ADONIS has enabled us to study the distribution of warm molecular hydrogen in the T Tauri system in considerably more detail than has been possible before. With multi-line observations it is possible to determine the excitation mechanism. The ratio of the (v = 1 – 0) S(1), (v = 2 – 1) S(1), and e.g. (v = 9 – 7) 0(3) near-IR lines can be taken to distinguish between UV fluorescence and shock excitation, and to determine the gas temperature in the latter case. From their integral field spectroscopy with 3D, Herbst et al. (1996) conclude that the bulk of the material is shock excited with a typical temperature of $\sim$ 2000 K. Future observations of the (v = 2 – 1) S(1) and (v = 9 – 7) O(3) with SHARP II and ADONIS could be used to map the gas temperature at higher spatial resolution, and to search for fluorescent H_2, whose presence is expected on the basis of IUE observations of UV fluorescence (Brown et al., 1981). Even more efficiently, such observations could be performed with the 3D integral field spectrometer, which will be coupled to the ALFA adaptive optics system on Calar Alto in the course of 1997. In addition to the multiplex advantage of 3D, the strictly simultaneous spectra will allow a much better continuum subtraction, and thus a better definition of the emission close to the two bright stars.

Acknowledgements

We thank the ESO staff on La Silla for their excellent support during our observing run. We are particularly indebted to Frank Eisenhauer, who built the SHARP II camera and calibrated its scanning Fabry-Perot etalon, for his expert advice on observing strategy and data reduction.

References

Artymowicz, P., & Lubow, S.H. (1996), *ApJ* **467**, L77.
Beckwith, S., Gatley, I., Matthews, K., & Neugebauer, G. (1978), *ApJ* **223**, L41.
Brown, A., Jordan, C., Millar, T.J., Gondhalekar, P., & Wilson, R. (1981), *Nature* **290**, 34.
Bührke, T., Brugel, E.W., & Mundt, R. (1986), *A&A* **163**, 83.
Carr, J.S. (1990), *AJ* **100**, 1244.
Dyck, H.M., Simon, T., & Zuckerman, B. (1982), *ApJ* **255**, L103.
Ghez, A.M., Neugebauer, G., Gorham, P.W., Haniff, C.A., Kulkarni, S.R., Matthews, K., Koresko, C., & Beckwith, S. (1991), *AJ* **102**, 2066.
Herbst, T.M., Beckwith, S.V.W., Glindemann, A., Tacconi-Garman, L.E., Kroker, H., & Krabbe, A. (1996), *AJ* **111**, 2403.
Koresko, C.D., Herbst, T.M., & Leinert, Ch. (1997), *ApJ*, in press.
Momose, M., Ohashi, N., Kawabe, R., Hayashi, M., & Nakano, T. (1996), *ApJ* **470**, 1001.
Nakajima, T., & Golimowski, D.A. (1995), *AJ* **109**, 1181.
Robberto, M., Clampin, M., Ligori, S., Paresce, F., Sacca, V., & Staude, H.J. (1995), *A&A* **296**, 431.
Schwartz, R.D. (1975), *ApJ* **195**, 631.
Smith, M. D., & Brand, P. W. J. L. (1990), *MNRAS* **242**, 495.
Solf, J., Böhm, K.-H., & Raga, A. (1988), *ApJ* **334**, 229.
van Langevelde, H.J., van Dieshoeck, E.F., van der Werf, P.P., & Blake, G.A. (1994), *A&A* **287**, L25.
Weintraub, D.A., Kastner, J.H., Zuckerman, B., & Gatley, I. (1992), *ApJ* **391**, 784.
Weintraub, D.A., Masson, C.R., & Zuckerman, B. (1989), *ApJ* **344**, 915.
Zinnecker, H., & Wilking, B.A. (1992), in *Binaries as tracers of Stellar Formation,* Eds. Duquennoy, A., & Mayor, M., Cambridge Univ. Press, p. 269.

Examples of High-Resolution Imaging and Polarimetry of R Monocerotis and NGC 2261

N. AGEORGES, J. R. WALSH, ESO

1. Introduction

High angular resolution polarisation and surface brightness images of R Monocerotis (R Mon) and its associated reflection nebulae NGC 2261 (Hubble's variable nebula), have been obtained. Ground-based optical imaging and near-infrared polarimetric data as well as HST optical polarisation measurements are presented as examples of current high-resolution imaging capabilities.

R Mon is a variable semi-stellar object, which has never been resolved into a single star. It is presumed to be a very young star in the process of emerging from its parent cloud and the source of illumination of the nebula. For decades the variability of both R Mon, and NGC 2261, has been observed both in brightness and polarisation (Hubble, 1916; Lightfoot, 1989). The apparent cometary nebula NGC 2261 extends, in the optical $\approx 3'$ northward of R Mon. CO mapping (Canto et al., 1981) reveals that it is indeed one lobe of a bipolar nebula; the southern lobe being obscured by the presumed tilted disk around R Mon. Some 7′ north of R Mon there are a group of associated Herbig-Haro objects (HH39). A faint loop extending between HH39 and the eastern extremity of NGC 2261 has been interpreted by Walsh & Malin (1985) as evidence of a stellar wind driven flow between R Mon and HH39. Imhoff & Mendoza (1974) derived a luminosity of 660 $L_\odot$ for R Mon, assuming a distance of 800 pc (Walker, 1964), which is atypical of the low luminosity normally observed for Herbig-Haro exciting sources. There is also a faint jet-like feature south of R Mon (Walsh & Malin, 1985); this is not a true jet but dust illuminated by radiation escaping from the dusty disk around R Mon (Warren-Smith et al., 1987).

In this article we present new observational data at high spatial resolution and discuss some possible explanations of the features revealed. These data serve to illustrate the state of the art in high angular resolution polarimetry. The observations have been acquired both from the ground with SUSI and ADONIS at ESO-Chile and from space with the Hubble Space Telescope. In section 2 we present in some detail the observational procedures. Some results are shown in section 3 and we end by a short discussion on R Mon and NGC 2261 together with some comments on the potential of high-resolution polarimetry.

2. Observations

NGC 2261 has been adopted as an HST polarisation calibrator (Turnshek et al., 1990), since it is extended, has high polarisation ($\gtrsim$ 10%) and has been well observed from the ground (see e.g. Aspin et al., 1985 and Minchin et al., 1991). The ADONIS and HST polarimetric data of R Mon and NGC 2261 presented here were acquired in order to calibrate polarimetric data of other